An Enhanced Receiver to Decode Superposed LoRa-Like Signals

Mohamed Amine Ben Temim, *Student Member, IEEE*, Guillaume Ferré, *Member, IEEE*, Baptiste Laporte-Fauret, *Graduate Student Member, IEEE*, Dominique Dallet, *Member, IEEE*, Bryce Minger, and Loïc Fuché

***Abstract*—To cope with the exponential rise of emerging technology, there have been significant developments in intelligent communication systems aimed at low-power and long-range wireless Internet-of-Things (IoT) communication. Among the various number of leading low-power wide-area network (LPWAN) technologies, long range (LoRa) has emerged to be an attractive solution to connect devices in free bands. Operating in unlicensed bands requires connected objects to reduce their energy consumption. To this end, one of the adopted techniques is random access to the radio channel, which leads to an increase in the probability of packet collisions. In this article, we propose a new receiver capable to decode several IoT LoRa-like signals simultaneously received with the same spreading factor which leads to destructive collisions. Based on the particular structure of the received signals and the successive interference cancellation (SIC) algorithm, we propose a novel approach to decode superposed LoRa-like signals iteratively. Simulations and real LoRa deployments are presented to validate the efficiency of our receiver.**

***Index Terms*—Collisions, Internet of Things (IoT), long range (LoRa), successive interference cancellation (SIC), synchronization.**

I. Introduction

THE DEPLOYMENT of the Internet of Things (IoT) involves many new challenges. Among them, energy consumption is paramount either from the economy than the ecological perspective. Indeed, according to IoT analytics study [1], the number of active IoT devices is expected to grow to 10 billion by 2020 and 22 billion by 2025. According to the same study, more than two billion devices will be connected through low-power wide-area networks (LPWANs) by 2025.

Manuscript received October 30, 2019; revised February 6, 2020 and March 13, 2020; accepted March 24, 2020. Date of publication April 8, 2020; date of current version August 12, 2020. This work was supported by the French State, managed by the French National Research Agency (ANR) in the frame of the "Investments for the Future" Programme IdEx Bordeaux-SysNum under Grant ANR-10-IDEX-03-02. *(Corresponding author: Mohamed Amine Ben Temim.)*

Mohamed Amine Ben Temim, Guillaume Ferré, and Dominique Dallet are with the University of Bordeaux, CNRS, Bordeaux INP, IMS, UMR 5218, 33400 Talence, France (e-mail: mohamed-amine.ben-temim@ims-bordeaux.fr; guillaume.ferre@ims-bordeaux.fr; loic.fuche@thalesgroup.com).

Baptiste Laporte-Fauret is with the University of Bordeaux, CNRS, Bordeaux INP, IMS, UMR 5218, 33400 Talence, France, and also with Thales, 92230 Gennevilliers, France (e-mail: baptiste.laporte-fauret@thalesgroup.com).

Bryce Minger and Loïc Fuché are with Thales, 92230 Gennevilliers, France (e-mail: bryce.minger@thalesgroup.com; loïc.fuché@thalesgroup.com).

Digital Object Identifier 10.1109/JIOT.2020.2986164

If the predictions of the exponential increase in the number of connected objects are confirmed, their density in urban areas will lead to a saturation of the electromagnetic spectrum in the free bands. Indeed, operating in free bandwidth, typically industrial, scientific, and medical (ISM) bands, offers the possibility to different devices to access the spectrum and provides a wide number of services as long they abide by regulations. The primary advantage is license cost effectiveness. Nevertheless, the main downside of uncontrolled channel access is packet collisions.

Many technologies are specifically designed to connect various objects to the Internet. Among them, long range (LoRa) [2] has emerged to be an interesting solution. LoRa technology was developed by a french company called Cycleo, and then acquired and patented by Semtech [2] which is at present selling LoRa chips. As explained in [3] and [4], LoRa is a spread spectrum technology and more precisely, it is the chirp spread spectrum (CSS) modulation [5] that is used to transmit binary information. This modulation technique requires the use of various spreading factors (SFs) to obtain orthogonal transmissions and reduce destructive collisions. In such configuration, destructive collisions occur only when two or more signals are simultaneously received in the same frequency band and with the same SF. Packet collisions are unavoidable in communication systems with random access to the channel such as LoRa-based networks. Yet, the processing of the latter collisions can be preventive or palliative. Among preventive approaches, we can mention the use of a random-access channel (RACH) in LoRaWAN [6]. In such configuration, if the nodes do not receive an acknowledgment, due to an out of range communication or the presence of interfering signals, they wait for a random period before transmitting again at the expense of spectral efficiency. In the same context, Ni *et al.* [7] proposed to reduce the occurrence of destructive collisions in LoRaWAN by using redundant gateways. However, in this article, we propose a palliative approach at the physical layer level. This processing allows us to reduce the number of retransmitted packets which will enhance the spectral efficiency.

In this article, we deal with an uplink communication case where several LoRa-like signals are simultaneously received over the same channel and with the same SF at the gateway. Due to the random access protocols adopted by LoRa-based networks and the deployment of low-cost crystal oscillators which have an inherent mismatch with their nominal

frequency, all the received signals are randomly desynchronized in time and suffer from carrier frequency offsets. The goal of this article is to design an efficient receiver capable to decode superposed LoRa-like signals in such configuration. Our approach is based on the successive interference cancellation (SIC) algorithm which is relevant because the interference can be removed efficiently based on the symbol estimation. The proposed algorithms are implemented at the gateway, which has generally no restriction on power consumption since it is continuously supplied.[1] This processing would reduce the energy consumption of the nodes and enhance their spectral efficiency since it decreases the number of retransmitted packets. Finally, to evaluate the performance of our receiver, we perform simulation using LoRa-like signals synthesized with MATLAB before considering real LoRa deployments.

This remainder of this article is organized as follows. In Section II, the related works are presented. Section III details the models of transmitted and received LoRa-like signals. Section IV presents our proposed algorithms to enhance the reception while Section V highlights the efficiency of the proposed approach on different simulations and real data results. Finally, Section VI presents conclusions and future prospects.

II. Related Works

In this section, we review existing works related to this article in order to highlight our contribution to face the problem of the same SF interference in LoRa.

Elshabrawy and Robert [8] and Afisiadis *et al.* [9] have analyzed the impact of the same SF interfering signal on the decoding performance of the signal of interest by presenting the theoretical models of the interference. This analysis is done at the expense of the interfering signal whose information is lost. This article does not propose any method to process the interference issue and thus decoding the colliding signals.

Simulators to evaluate the impact of same and different SF interference on LoRaWAN performance are implemented in [10] and [11]. The authors showed that different SF is not perfectly orthogonal and such collision can lead to a packet loss if the signal-to-interference ratio (SIR) is lower than a threshold value for each SF configuration. Moreover, for the same SF collisions and by using the capture effect, they assumed that the signal of interest is well decoded if its power is 6 dB greater than the total power of the interfering signals. These papers allow us to know the limits of our method but in no way propose solutions to treat interference as we suggest in this article.

In a similar context, Noreen *et al.* [12] studied the capture effect (i.e., define the SIR threshold allowing the accurate decoding of the signal of interest) and proposed to use the SIC algorithm to decode the superposed signals. However, this analysis does not provide any explanation about how the interference cancellation and the synchronization are performed. They presented the throughput of the proposed system using an abstraction of the physical layer since they assumed that the SIC is well performed if the SIR is greater than a threshold value.

TABLE I
Related Works Comparison

KPI / Papers	Frequency synchronization algorithm	Time synchronization algorithm	Interference cancellation algorithm	Decoding performance algorithm
[8], [9]	✗	✗	✗	Only the strongest signal
[10], [11]	✗	✗	✗	Only the strongest signal
[12]	✗	✗	✓	Not precised
[13]	✗	✗	✗	Only 2 superposed signals
[14]	✗	✓	✓	Only 2 superposed signals
Our paper	✓	✓	✓	All superposed signals

A novel approach to decode nonorthogonal LoRa signals using the specific structure of the chirps is presented in [13]. However, their proposed algorithms could decode only two superposed signals and require the receiver to be perfectly synchronized or slightly desynchronized which is unrealistic in a random access scenario as adopted by LoRa-based networks. In addition, using the spectrogram[2] of the chirps to decode the superposed signals is not very efficient since it requires a good signal-to-noise ratio (SNR) to identify them. Basically, the problems occur when we are close to the receiver sensitivity.

Finally, we already dealt in [14] with an uplink case where two desynchronized LoRa-like signals are simultaneously received on the same channel and with the same SF. We proposed an approach based on the fast Fourier transform (FFT) representation to decode both signals. However, we assumed that the signal having the highest power was received first which is not always the case. Our contribution to this article can be viewed as a generalization of this article.

Based on this, to the best of our knowledge, there is no work that deals with the same SF interference by considering almost a real-world scenario (i.e., random time and frequency desynchronization). Indeed, we provide mathematical models allowing us to develop our novel approach to face this interference issue. Furthermore, using a simple implemented SIC algorithm makes this article easily testable in the current LoRa chip which we have proved in Section V-B.

We propose to summarize this state of the art in Table I.

III. System Model

We consider an uplink communication system where several LoRa-like signals are supposed to be simultaneously received on the same channel and with the same SF. Indeed, those signals come from IoT LoRa nodes transmitting data to a gateway

[1]It should be noted that without power consumption constraints, the proposed algorithms can also be implemented on the nodes.

[2]A spectrogram is a visual representation of the spectrum of frequencies of a signal as it varies with time.

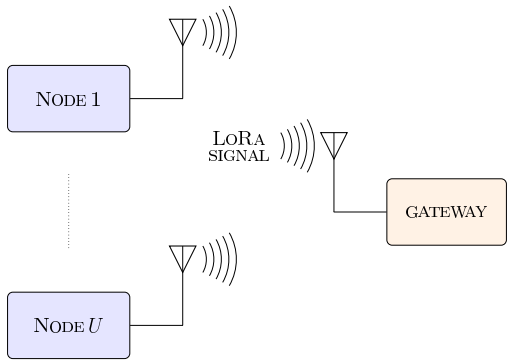

Fig. 1. Test bed for U LoRa transmissions simultaneously received by the gateway.

TABLE II
NOTATIONS AND DEFINITIONS

Notations	Definitions
T	symbol time
$M = 2^{SF}$	total symbol number
$B = \frac{2^{SF}}{T}$	signal bandwidth
$f(t) = \frac{B}{T}t, \forall t \in [-\frac{T}{2}, \frac{T}{2})$	raw chirp
T_s	sampling time
U	number of superposed signals
$\mathbb{1}_{[0,x)}(t)$	the indicator function
$x \mod M$	the modulo M operation of x
$\lfloor . \rfloor$ / $\lceil . \rceil$	flooring/rounding operation

as depicted in Fig. 1. As presented in [15], receiving simultaneously two or more signals with the same SF leads to a loss of orthogonality and may cause the loss of all packets.

In the remainder of this article, we consider the notations and definitions listed in Table II.

A. Presentation of the Transmitted LoRa Signals

In this section, we present the structure of the signals transmitted by LoRa nodes. For more details on the LoRa physical layer, readers can refer to [9], [15], and [16].

1) LoRa PHY Layer Principle: As we mentioned, LoRa is a spread spectrum technology derived from the CSS modulation. Indeed, for each node $i \in \{1, \ldots, U\}$, we define $f_i(t - pT)$ as the transmitted chirp $\forall t \in [pT - (T/2), pT + (T/2)]$. This chirp is obtained using $\gamma_i(p) = ([m_i(p)]/B)$ and performing a cyclic shift as depicted by Fig. 2. It should be noted that $m_i(p)$ corresponds to the transmitted symbol at time pT. It is a random value uniformly distributed in $[\![0, M-1]\!]$ and is obtained from the binary to decimal conversion of SF bits.

$f_i(t - pT)$ can be expressed as the derivative of its phase $\phi_i(t - pT)$

$$f_i(t - pT) = \frac{1}{2\pi}\frac{\mathrm{d}\phi_i(t - pT)}{\mathrm{d}t}. \tag{1}$$

Thus, we obtain for $t \in [pT - (T/2), pT + (T/2) - \gamma_i(p))$

$$\phi_i(t - pT) = 2\pi\left[\frac{B}{2T}t^2 + \frac{m_i(p)}{T}t\right]. \tag{2}$$

For $t \in [pT + (T/2) - \gamma_i(p), pT + (T/2))$

$$\phi_i(t - pT) = 2\pi\left[\frac{B}{2T}t^2 + \left(\frac{m_i(p)}{T} - B\right)t\right]. \tag{3}$$

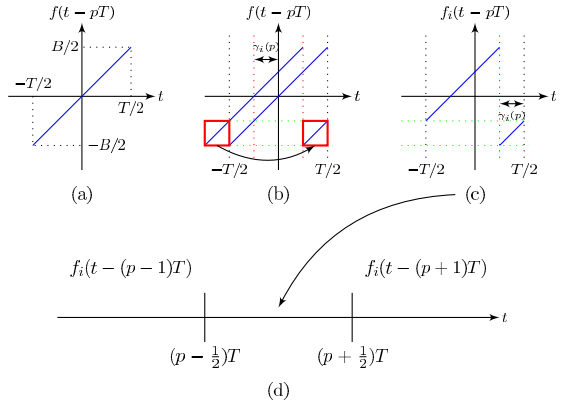

Fig. 2. Symbol → chirp association process. (a) Up raw chirp. (b) Process principle. (c) Associated chirp. (d) Temporal location of the chirp.

If we note $x_i(t)$, the complex envelope of the signal transmitted by the ith LoRa node, we have

$$x_i(t) = \sum_{p\in\mathbb{Z}} e^{j\phi_i(t-pT)}. \tag{4}$$

After giving a brief overview of the LoRa physical layer and its CSS modulation, we dedicate the next paragraph to detail the LoRa frame structure.

2) LoRa Frame Structure: As defined in [17], the LoRa frame is composed of the following.

1) A preamble with a number N_p of up raw chirp symbols which are exploited to detect the presence of LoRa signal [18].
2) A word of synchronization called a "sync word" which is constituted of two special modulated symbols [19]. It is used for the timing frame synchronization to convey the end of the preamble to the receiver and thus, to know the effective start of the frame.[3]
3) A start of the frame delimiter (SFD) which is composed of 2.25 down chirps that could be used for the frequency synchronization.
4) A PHY-header containing the frame information, a variable-length PHY-payload and a cyclic redundancy check (CRC).

As highlighted in [17], the PHY-header and the CRC are optional. The previous structure of a LoRa frame is illustrated in Fig. 3, which is obtained by recording real LoRa data using our own-made nodes as we will present in Section V-B.

3) LoRa Frame Generation: The signal transmitted by each LoRa node is started by the aforementioned preamble, the sync word, and the SFD. Then, its stream of data is generated in the form of N_s^i symbols that are uniformly distributed in $[\![0, M-1]\!]$.

Based on the LoRa frame structure, a realistic complex envelope of the signal transmitted by the ith node can be written as

$$s_i(t) = \sum_{p=0}^{N_p-1} e^{j\phi(t-pT)} + \sum_{p=N_p}^{N_p+1} e^{j\tilde{\phi}_p(t-pT)}$$

[3]It also can be used to distinguish between devices from different networks. Indeed, if the sync word of the received packet does not match with the one configured in the gateway, then the gateway will stop receiving this packet.

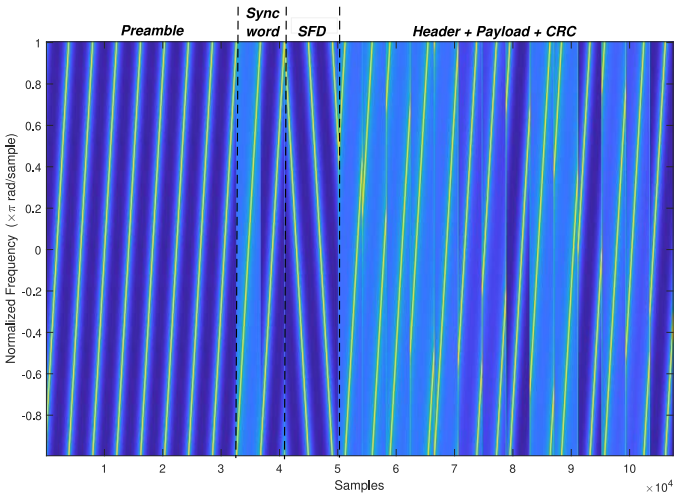

Fig. 3. Spectrogram of the LoRa frame obtained by recording real LoRa data.

$$+\sum_{p=N_p+2}^{N_t} e^{-j\phi(t-pT)} + \sum_{p=N_t+1}^{N_s^i+N_t-1} e^{j\phi_p^i(t-pT)} \quad (5)$$

where $N_t = N_p + 4.25$ is the total number of symbols of the preamble, synch word, and SFD and $\tilde{\phi}_p(t-pT)$ (resp. $\phi(t) = 2\pi(B/2T)t^2$), $t \in [pT-(T/2), pT+(T/2))$, is the instantaneous phase corresponding to a specific modulated symbols of the sync word (resp. raw chirp).

B. Received Signals at the Gateway

In this section, we detail the mathematical models and the demodulation principle of the received signals at a LoRa gateway. Due to the complete lack of synchronization between the gateway and the nodes, the continuous-time version of the received signal, when several LoRa-like frames with the same SF are superposed, can be written as

$$y(t) = \sum_{i=1}^{U} \sqrt{P_i} s_i(t-\Delta t_i) e^{-j(2\pi \Delta f_i t - \theta_i)} + w(t) \quad (6)$$

where P_i, θ_i, Δt_i, and Δf_i are the power, the initial phase, the time desynchronization, and the frequency offset of the ith received signal, respectively, and $w(t)$ is the complex additive white Gaussian noise (AWGN) signal with σ_w^2 as its variance.

We consider at first a reception case of one signal without any interference to explore the LoRa demodulation principle and then interfering signals are analyzed. We point out that all the processing is done at the gateway using the discrete version of the received signals and time and frequency synchronizations are needed before decoding their information.

1) Case Without Interference ($U = 1$): Similar to any other modulation mechanism, the decoding process of LoRa-like signals requires an accurate time and frequency synchronizations. Hence, the received signal synchronized on node 1 frame and sampled at $T_s = (1/B)$ is given by

$$y(n) = \sqrt{P_1} s_1(n) + w(n) \quad (7)$$

with $w(n)$ being the discrete-time version of the noise.

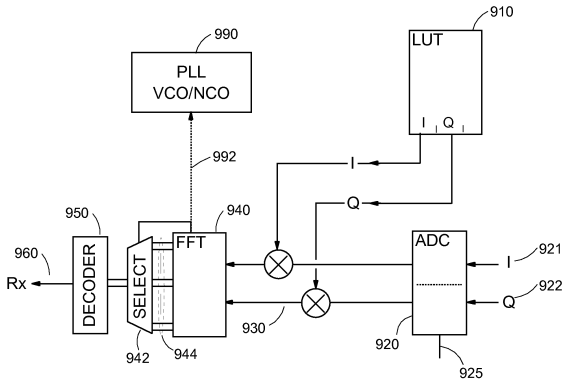

Fig. 4. LoRa receiver architecture [20, Fig. 9].

The transmitted symbols are detected by multiplying each T-long section of the received signal by complex envelope corresponding to the conjugate of the raw chirp (i.e., down-chirp signal). Based on the principle of the LoRa-Like symbol detection detailed in [17] and [20] and Fig. 4, the signal obtained after the FFT processing of the pth symbol of node 1 without any interfering signals, can be expressed as

$$Y(k,p) = \frac{1}{\sqrt{M}} \sum_{n=0}^{M-1} y(nT_s + pT) e^{-j\phi(nT_s+pT)} e^{-j2\pi \frac{nk}{M}} \quad (8)$$

with $k \in [\![0, M-1]\!]$, thus based on [15] and after some calculations

$$Y(k,p) = \sqrt{P_1 M}\delta(k - m_1(p)) + W(k,p) \quad (9)$$

where $\delta(k)$ represents the Kronecker impulse and $W(k,p) \sim \mathcal{N}_{\mathbb{C}}(0, \sigma_w^2)$ is the FFT of the noise.
The estimation of the symbol $m_1(p)$ is done by looking for the frequency k that maximizes the module of (9).

2) Case of Superposed Signals ($U > 1$): To detect, synchronize, and decode LoRa-like signals, the gateway has to be in a listening status. To this end, the received signals are sampled and multiplied by a train of down-chirp signals. It should be noted that this step is called the de-chirping operation in [21]. Indeed, the multiplication by the de-chirping sequence is performed, not necessarily in a synchronized mode at first since the beginning instant of each packet is not known in advance by the receiver. A practical method to perform accurate time and frequency synchronizations of the received signals is proposed in Section IV.

Based on Fig. 5, the de-chirping sequence, sampled at T_s, can be expressed as

$$d(n) = \sum_{p \in \mathbb{Z}} e^{-j\phi(nT_s - pT)}. \quad (10)$$

As the processing of LoRa-like signals at the gateway is done after the analog-to-digital converter (ADC), the discrete-time version of the received signal sampled at T_s is given by

$$y(n) = \sum_{i=1}^{U} \sqrt{P_i} s_i(n - \Delta n_i) e^{-j(2\pi \Delta f_i n T_s - \theta_i)} + w(n). \quad (11)$$

The discrete time shift Δn_i between the beginning of the de-chirping sequence and each superposed LoRa signal is

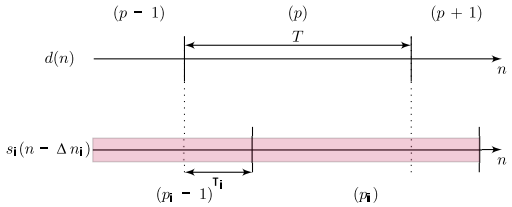

Fig. 5. LoRa-like symbol detection principle.

expressed as: $\Delta n_i = [(\Delta t_i)/T_s] = K_i M + \tau_i$ with $K_i \in \mathbb{N}$ and τ_i denoting the relative time offset between the ith signal with the de-chirping sequence and following the uniform distribution $\mathcal{U}[0, M)$. τ_i cannot be constrained to an integer value, since supposing that the de-chirping sequence is sample aligned with the received signals is not realistic. Therefore, this time offset is given by $\tau_i = \lfloor \tau_i \rfloor + \epsilon_i$, $\epsilon_i \in [0, 1)$.

Based on the principle of the LoRa-Like symbol detection detailed in [9], [15], and [17] and in Fig. 5, the signal obtained after the FFT, which corresponds to the processing of the pth T-long section of the de-chirping sequence is equal to

$$Y(k,p) = \frac{1}{\sqrt{M}} \sum_{n=0}^{M-1} \underbrace{(y(n,p)d(n,p))}_{z(n,p)} e^{-j2\pi \frac{nk}{M}} \tag{12}$$

where $y(n,p) = y(n)$ and $d(n,p) = d(n)$ $\forall n \in [\![pM, (p+1)M - 1]\!]$. Thus, based on [15], [22], Fig. 5, and after some calculations, we obtain

$$\begin{aligned} z(n,p) &= \sum_{i=1}^{U_p} z_{\tau_i}(n,p) + w(n) \\ &= \sum_{i=1}^{U_p} \Bigg(\sqrt{P_i} e^{j\left(2\pi n \frac{\bar{m}_i(p_i-1)}{M} + \phi^{p_i-1}\right)} \mathbb{1}_{[\![0, \lfloor \tau_i \rfloor]\!]}(n) \\ &\qquad + \sqrt{P_i} e^{j\left(2\pi n \frac{\bar{m}_i(p_i)}{M} + \phi^{p_i}\right)} \mathbb{1}_{[\![\lfloor \tau_i \rfloor + 1, M-1]\!]}(n) \Bigg) \\ &\quad + w(n) \end{aligned} \tag{13}$$

where

1) $U_p \in \{1, \ldots, U\}$ is the number of received signals in the pth T-long section of the de-chirping sequence;
2) ϕ^{p_i}, $p_i \in \{1, \ldots, N_t + N_s^i\}$, is the initial phase of the ith received signal in its p_i^{th} T-long section;
3) $\bar{m}_i(p_i)$, $p_i \in \{1, \ldots, N_t + N_s^i\}$, is the frequency of the detected peak of latter signal in a nonsynchronized mode. The relation between $\bar{m}_i(p_i)$ and the symbol initially transmitted is expressed as

$$\bar{m}_i(p_i) = m_i(p_i) - \lfloor \tau_i \rfloor - \lfloor \Delta f_i T \rceil \mod M. \tag{14}$$

Based on the structure of the ith de-chirped signal $\forall i \in \{1, \ldots, U\}$, we can observe that the FFT of a nonsynchronized signal gives two cardinal sines. Here, we notice that the maximum number of peaks that could be detected is $2 \times U_p$ depending on the positions of the latter peaks (probability of two superposed peaks) and the noise level of each signal. Therefore, in a nonsynchronized mode, accurate decoding of these signals is impossible.

TABLE III
TIME AND FREQUENCY DESYNCHRONIZATIONS IMPACTS ON FFT REPRESENTATION OF THE SYMBOL TO ESTIMATE

Synchronization	Observations after the FFT processing
$\tau_i \neq 0, \Delta f_i = 0$	Tow cardinal sines shifted by τ_i
$\tau_i = 0, \Delta f_i \neq 0$	One cardinal sine shifted by $\Delta f_i T$
$\tau_i \neq 0, \Delta f_i \neq 0$	Tow cardinal sines shifted by $\tau_i + \Delta f_i T$

In the next section, we propose a novel approach to detect, synchronize, and decode the maximum number of nonorthogonal signals simultaneously received.

IV. PROPOSED ALGORITHMS TO PROCESS THE RECEPTION OF MULTIPLE NONORTHOGONAL LORA-LIKE SIGNALS

In this section, we propose to design an enhanced receiver able to synchronize and decode simultaneously received nonorthogonal LoRa-like signals. Our approach consists of processing LoRa signals in a given time window. Indeed, the receiver sets a constant block duration T_B and tries to iteratively decode the maximum number of signals received along with this duration. The principle consists in:

1) detecting the received signals and identifying the strongest one;
2) decoding the strongest signal information;
3) reproducing its complex envelope and removing it from the received signal (SIC algorithm).

The latter operations are repeated until there is no detected LoRa-like signal left. We point out that every two consecutive blocks are overlapped by at least a maximum packet duration[4] to ensure the processing of all the received signals information.

A. Strongest Signal Synchronization Algorithms

Our algorithms aim to detect the effective start of the sth received signal, which corresponds to the strongest signal and to compensate its frequency offset Δf_s. To this end, we propose a coarse and fine synchronization.

1) Coarse Synchronization Based on Preamble Detection: The detection of the presence of LoRa-like signals is performed by a gateway in a listening mode. This is done by continuously de-chirping the sampled received signals. After that, an FFT is processed in each T-long section as presented in (12). Based on (13), the contributions of a LoRa-like signal in a T-long section, for different desynchronization scenarios, are given in Table III.

Nevertheless, given that all the symbols of LoRa preamble are equal to zero. Thus, only one peak is detected even in a nonsynchronized mode (time and frequency desynchronizations) since the contribution of two consecutive zero symbols would be superposed in the same FFT bin as depicted in Fig. 6 for the strongest signal. Thereby, given that $\forall p_s \in \{1, \ldots, N_p\}, m_s(p_s) = 0$ and by using (14), a nearly accurate estimation of the total shift of the main peak $\hat{\tau}_s' = \tau_s + \Delta f_s T$ can be easily performed.

Given the structure of LoRa packet preamble, averaging the module squared of the FFTs over each N_p T-long sections

[4]As an example, in LoRaWAN, the maximum packet duration is known for each SF.

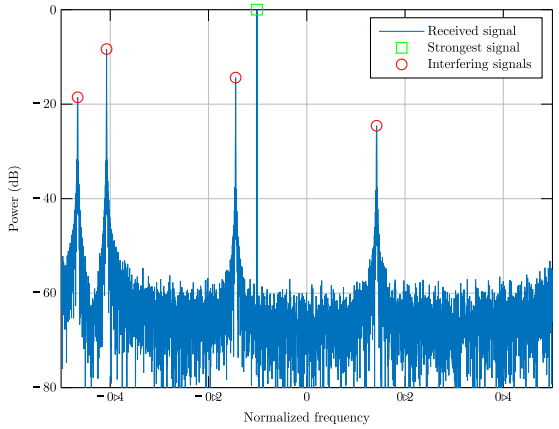

Fig. 6. Result of the FFT processing when the preamble of the strongest signal is superimposed with two interfering signals ($U_p = 3$).

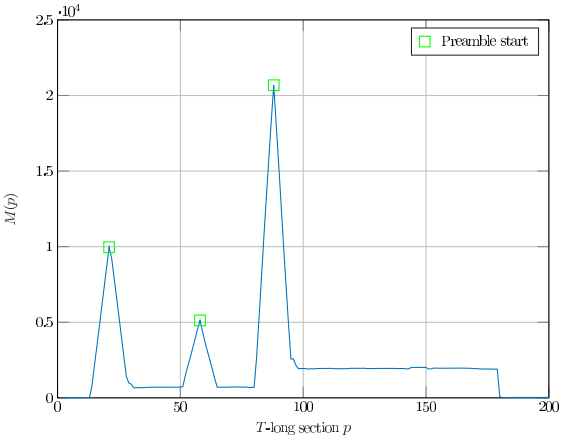

Fig. 7. Preamble detection process ($U = 3$).

would increase the certainty of preamble detection. If we note $T(k,p)$, $k \in [\![0, M-1]\!]$, $p \in \{1,\dots,N_B\}$ and $N_B = \lfloor (T_B/T) \rfloor$, the averaging function, we have

$$T(k,p) = \sum_{j=p}^{p+N_p-1} \left| \frac{Y(k,j)}{\sigma_w} \right|^2. \tag{15}$$

It should be noted that the estimation of the AWGN variance σ_w^2 is done on silent periods when no signal is received.

To coarsely estimate the index $\hat{K}_s$ of the T-long section that corresponds to the beginning of the strongest signal preamble, we compute the function $M(p)$, as presented in Fig. 7 when three signals are simultaneously received. This function represents the maximum value of $T(k,p)$ $\forall p \in \{1,\dots,N_B\}$

$$M(p) = \max_k (T(k,p)). \tag{16}$$

Then, if we note $\hat{K}_s$ an estimation of K_s, we have

$$\hat{K}_s = \underset{p}{\operatorname{argmax}}(M(p)). \tag{17}$$

We notice that, in each iteration of our algorithm, the identification of the maximum of $M(p)$ requires the definition of a threshold value to detect the existence of LoRa-like signals in the data block. This value is set using a classical hypothesis test on $T(k,p)$ according to the noise level.

Knowing that the FFT of the noise in the pth T-long section $W(k,p)$, $k \in [\![0, M-1]\!]$, follows the normal distribution $\mathcal{N}_{\mathbb{C}}(0,\sigma_w^2)$. Thus, it is easy to demonstrate that $\sum_{j=p}^{p+N_p-1} |([W(k,j)]/[\sigma_w])|^2$ follows the chi-squared distribution $\chi^2(.;N_p)$ with N_p as the degree of freedom.

If we note P_{fa}, the probability of the false alarm and we define hypothesis tests:

1) $\mathcal{H}_0$: $\{U_j = 0 \quad \forall j \in \{p,\dots,p+Np\}\}$;
2) $\mathcal{H}_1$: $\{\exists j \in \{p,\dots,p+Np\}, U_j \neq 0\}$.

We have

$$\begin{aligned} P_{fa} &= P\big[\mathcal{H}_1/\mathcal{H}_0\big] \\ &= P\Big[T(k,p) > \mathrm{Th}/T(k,p) \sim \chi^2\big(.;N_p\big)\Big] \\ &= 1 - P\Big[T(k,p) < \mathrm{Th}/T(k,p) \sim \chi^2\big(.;N_p\big)\Big] \\ &= 1 - F_{\chi^2}\big(\mathrm{Th};N_p\big) \end{aligned} \tag{18}$$

where $F_{\chi^2}(.;N_p)$ is the cumulative density function of the chi-squared distribution with N_p degree of freedom.

Thus, the threshold Th could be expressed as

$$\mathrm{Th} = F_{\chi^2}^{-1}\big(1 - P_{fa};N_p\big). \tag{19}$$

Therefore, if $T(k,p) < \mathrm{Th} \quad \forall p \in \{1,\dots,N_B\}$, no LoRa-like signal is detected in the considered block.

2) Fine Synchronization Based on the SFD: The previous synchronization procedure has enabled the detection of the strongest received signal and the estimation of K_s and τ_s'. However, due to the random distribution of the total shift τ_s' (caused by τ_s and Δf_s), we will have a significant uncertainty on the estimation of K_s. Furthermore, to estimate the time shift τ_s, it is mandatory to compensate the frequency shift. As a consequence, we propose a fine frame synchronization procedure in order to reduce the latter uncertainty and to compensate the frequency offset Δf_s.

To the same end, Colavolpe *et al.* [21] used a local correlation with the preamble and the sync word, whereas Knight and Seeber [23] proposed to perform a framing of the SFD by increasing the time-based FFT resolution. Here, we suggest an optimized method based also on the SFD framing. It is simply needed to compensate the total shift $\hat{\tau}_s'$ and apply an up-chirp sequence to the T-long sections where the down-chirp symbols of the SFD are expected. The two highest successive FFTs maxima in the same FFT bin indicate the beginning of the down chirps. Hence, an accurate estimation of K_s can be performed.

After the latter up-chirping operation, the SFD down-chirp symbols must be decoded with a zero value in the case of accurate time and frequency synchronizations. However, due to the frequency offset, the latter symbols are shifted as depicted in (14) and in Table III.

If we note $\hat{m}_s'$ and $\bar{m}_s'$, the detected FFT argmax of a down-chirp symbol after and before compensating $\hat{\tau}_s'$, respectively, and m_s the transmitted down-chirp symbol, we have

$$\begin{aligned} \hat{m}_s' &= \bar{m}_s' - \hat{\tau}_s' \mod M \\ &= m_s + \tau_s - \Delta f_s T - \tau_s - \Delta f_s T \mod M \\ &= m_s - 2\Delta f_s T \mod M. \end{aligned} \tag{20}$$

TABLE IV
SNR THRESHOLDS FOR LORA-LIKE SIGNAL WITH $B = 125$ kHz

SF	7	8	9	10	11	12
$\Gamma_{th}^{(SF)}$ (dB)	-6	-9	-12	-15	-17.5	-20

Given that $m_s = 0$ and by estimating down-chirp symbols after compensating $\hat{\tau}_s'$, we can easily deduce the frequency offset Δf_s and compensate it. However, this estimation is biased since the latter offset cannot be constrained to an integer value. Therefore, an interpolation is performed around the FFT maximum sample to refine the search.

Finally, after the estimation of τ_s' and Δf_s, the time offset $\hat{\tau}_s$ could be easily deduced.

B. Decoding the Strongest Signal

Once the receiver is synchronized to the beginning of the frame of the signal having the highest received power, a synchronized de-chirping process is applied to it. Consequently, an FFT is performed for each T-long section of the latter frame.

If we note $z_s(n, p_s)$ the de-chirped received signal synchronized on the strongest signal, we have

$$z_s(n,p_s) = \sqrt{P_s} e^{j\left(2\pi n \frac{m_s(p_s)}{M} + \phi^{p_s}\right)} + \sum_{i=1}^{U_{p_s}-1} z_{\tau_i^s}(n,p_s) + w(n) \tag{21}$$

with $n \in [\![\Delta n_s + p_s M, \Delta n_s + (p_s+1)M - 1]\!]$ and τ_i^s being the time offset between the synchronized signal and the ith interfering signal. Using (12) and some calculation, the FFT of $z_s(n, p_s)$ can be expressed as

$$Y_s(k,p_s) = \sqrt{P_s M}\delta(k - m_s(p_s)) + \sum_{i=1}^{U_{p_s}-1} Y_i(k,p_s) + W(k) \tag{22}$$

where $Y_i(k, p_s)$ is the FFT of the ith signal interfering the decision of the p_s^{th} symbol. Hence, the estimation of the p_s^{th} transmitted symbol is obtained as

$$\hat{m}_s(p_s) = \underset{k}{\operatorname{argmax}}\left(|Y^s(k,p_s)|\right). \tag{23}$$

In this context, several works have evaluated LoRa-like signal decoding performance. Elshabrawy and Robert [8] and Afisiadis *et al.* [9] presented the bit error rate (BER) curves of LoRa signals (with and without same-SF interference) as a function of the SNR. The later is equal to (P/σ_w^2) where P represents the power of the received signal. Then, Elshabrawy and Robert [8] demonstrated that the SNR thresholds $\Gamma_{\text{th}}^{(SF)}$, necessary to guarantee the coverage characterized by LoRa network without interference, are those associated to a BER of 10^{-5}. The values of these SNR thresholds are given in Table IV.

They showed also that the SNR thresholds are affected in the presence of a same SF interference and proved that the decoding performance of the signal of interest is slightly affected if its power is at least 6 dB greater than the power of the interfering signal.

C. Strongest Signal Cancellation

Once the receiver is synchronized on the strongest signal, it estimates the frequency as presented in (23), the magnitude and the phase of the main peak in each T-long section of the later signal. Then, the associated symbols are decoded and the signal could be reproduced in each symbol section and subtracted from the received signal.

If we note $\hat{z}_s(n, p_s)$ the reconstruction of the synchronized signal, in the p_s^{th} T-long section, synthesized by the estimation of its frequency $\hat{m}_s(p_s)$, magnitude $\sqrt{\hat{P}_s^{p_s}}$, and initial phase $\hat{\phi}^{p_s}$, we have

$$z(n,p_s) = z(n,p_s) - \hat{z}_s(n,p_s) \tag{24}$$

where $\hat{z}_s(n, p_s)$ is expressed as

$$\hat{z}_s(n,p_s) = \sqrt{\hat{P}_s^{p_s}} e^{j\left(2\pi n \frac{\hat{m}_s(p_s)}{M} + \hat{\phi}^{p_s}\right)}. \tag{25}$$

In the same context, Noreen *et al.* [12] proved that the SIC could be performed only if the power ratio between the strongest signal and the weak one is at least 1 dB.

D. Processing of Superimposed Peaks

Dealing with simultaneously received LoRa-like signals with the same SF causes some critical cases that should be studied to avoid the degradation of the decoding performance. As presented in (21), after the FFT processing, the synchronized signal contributes by one Dirac at the symbol to estimate, but the other existent signals contribute by two cardinal sines each. As a result, there is a nonnull probability that one of these peaks is located at the same FFT bin with the Dirac of the synchronized signal. In this case, after estimating the frequency, magnitude, and phase of the main peak, the latter is removed and then the contribution of the other existent signals in the same FFT bin is also reduced.

To address this issue, we propose to compare the magnitude of the current FFT main peak with a mean value, denoted as $\sqrt{\bar{P}_s}$ and computed from the main peaks in all the T-long sections of the signal of interest. If this current magnitude is considerably greater than the mean value, two or more superposed peaks are assumed to be detected. In this case, a hypothesis test is done by referring to the distribution of the demodulation metric $|Y_s(k, p_s)|$. Thus, if we suppose that there are no interfering signals in the p_s^{th} T-long section and by using the basic properties of the complex normal distribution, we have

$$|Y_s(k,p_s)| \sim \begin{cases} \mathcal{R}_i\left(\sqrt{P_s M}, \sigma_w\right), & \text{for } k = m_s(p_s) \\ \mathcal{R}_i(0,\sigma_w), & \text{else} \end{cases} \tag{26}$$

where $\mathcal{R}_i(u, v)$ is the Rician distribution with u and v are the location and the scale parameters.

In this case, we define the hypothesis of our test as follows.

1) $\mathcal{H}_0$: One peak exists at the FFT bin of the symbol to be decoded.
2) $\mathcal{H}_1$: Two or more peaks are superposed at the FFT bin of the symbol to be decoded.

Using the same definition of the probability of false alarm $P_{fa}^{'}$ as we detailed in Section IV-A1, we can easily deduce the

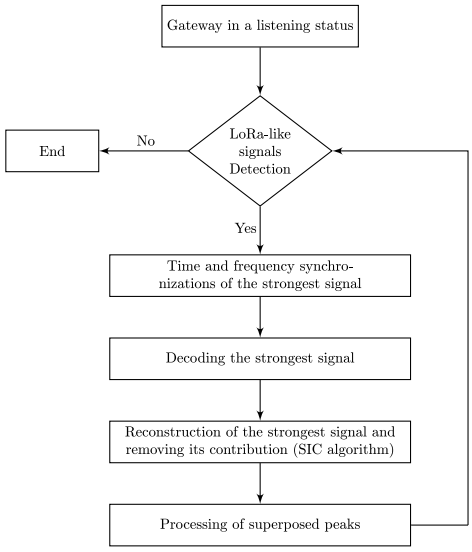

Fig. 8. Adopted algorithm.

value of the threshold allowing the detection of two or more peaks at the FFT bin of the symbol to be decoded

$$\mathrm{Th}^{'} = F_{\mathcal{R}_i}^{-1}\Big(1 - P_{fa}^{'}; \sqrt{P_s M}, \sigma_w\Big). \tag{27}$$

Once the receiver detects the presence of two or more peaks at the FFT bin of the current symbol of the synchronized signal, the magnitude and the phase of the reconstructed signal in (25) will be $\sqrt{\bar{P}_s}$ and $\bar{\phi}$, where $\bar{\phi}$ is the mean phase computed from the initial phases in all the T-long sections. It should be noted here that LoRa modulation is a memoryless continuous phase modulation [15]. Thus, the initial phases are equal in all the T-long sections.

Thereby, this operation allows to maintain the contribution of the signals other than the strongest one in the same FFT bin.

Finally, as depicted in Fig. 8, which summarizes the adopted approach to design our receiver, the algorithms in Sections IV-A–IV-D are repeated until no LoRa-like signal is detected in the considered block. The reader can find more details about our algorithm in Algorithm 1.

In the next section, the performance of our receiver is evaluated through MATLAB simulation and real LoRa deployments.

Algorithm 1: Decoding Superposed LoRa-Like Signals

Input: $y(n)$, SF, B, N_B
$M \leftarrow 2^{SF}$.
$z(n,p) \leftarrow (13)$, $n \in [\![pM, (p+1)M-1]\!]$ and $p \in \{1,\ldots,N_B\}$ (dechirping operation).
$Y(k,p) \leftarrow (12)$, $k \in [\![0, M-1]\!]$ (FFT).
$T(k,p) \leftarrow (15)$ (averaging function).
$M(p) \leftarrow \underset{k}{max}(T(k,p))$.
$Th \leftarrow (19)$ (noise threshold).
while $\exists p \in \{1,\ldots,N_B\}, M(p) > Th$ **do**
  $\hat{K}_s \leftarrow \underset{p}{argmax}(M(p))$.
  $\hat{\tau}_s, \hat{\Delta}f_s \leftarrow$ fine synchronization (section IV-A2).
  $\Delta n_s \leftarrow \hat{K}_s M + \hat{\tau}_s$.
  for $p_s \leftarrow 1$ *to Nsymbols* **do**
    $z_s(n,p_s) \leftarrow (21)$, $n \in [\![\Delta n_s + p_s M, \Delta n_s + (p_s+1)M - 1]\!]$.
    $Y^s(k,p_s) \leftarrow FFT(z_s(n,p_s))$.
    $\hat{m}_s(p_s) \leftarrow \underset{k}{argmax}(|Y^s(k,p_s)|)$ (estimated symbol).
    $\sqrt{\hat{P}_s^{p_s}} \leftarrow \underset{k}{max}(|Y^s(k,p_s)|)$ (estimated magnitude).
    $\hat{\phi}^{p_s} \leftarrow arg(|Y^s(\hat{m}_s(p_s),p_s)|)$ (estimated phase).
    $Th' \leftarrow (27)$ (threshold to detect superposed signals).
    if $\sqrt{\hat{P}_s^{p_s}} > Th'$ **then**
      $\hat{A}_r \leftarrow \underset{p_s}{mean}(\sqrt{\hat{P}_s^{p_s}})$.
      $\hat{\phi}_r \leftarrow \underset{p_s}{mean}(\hat{\phi}^{p_s})$
    else
      $\hat{A}_r \leftarrow \sqrt{\hat{P}_s^{p_s}}$.
      $\hat{\phi}_r \leftarrow \hat{\phi}^{p_s}$.
    end
    $\hat{z}_s(n,p_s) \leftarrow \hat{A}_r e^{j\left(2\pi n \frac{\hat{m}_s(p_s)}{M} + \hat{\phi}_r\right)}$ (reconstruction of the strongest signal).
    $z(n,p_s) \leftarrow z(n,p_s) - \hat{z}_s(n,p_s)$ (SIC).
  end
  $T(k,p) \leftarrow (15)$.
  $M(p) \leftarrow \underset{k}{max}(T(k,p))$.
end

V. Results and Discussion

In this section, we aim to evaluate the performance of our receiver to synchronize and decode simultaneously received LoRa-like signals with the same SF. To this end, we propose to:

1) perform Monte Carlo-based simulations using synthesized LoRa-like signals;
2) use own-made LoRa nodes and gateways to validate our results with real LoRa deployments.

A. Simulation Results on Synthesized Signals

1) Considered Scenario: The considered scenario consists of simultaneously receiving U LoRa-like signals at random arrival instants using the parameters in Table V. The packets are generated using our MATLAB simulator and have the structure as presented in Section III-A. For the sake of simplicity, we assumed that the simulated receiver is aware of the packet and the preamble lengths.

TABLE V
Simulation Parameters

Bandwidth (kHz)	125
Spreading Factor	$\{12; 9\}$
Frame length	$80\times T$
Block length T_B	$200\times T$
Preamble length N_p	8
Number of superposed signals U	$\{2; 3; 4\}$
Number of Monte Carlo iterations	10000

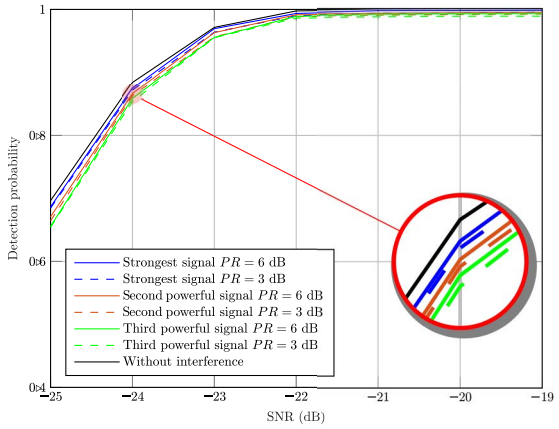

Fig. 9. Start of frame detection with $SF = 12$ and $U = 3$.

In the following, we define the power ratio between each two received signals:

$$\left(\mathrm{PR}_{i,j}\right)_{\mathrm{dB}} = 10\log_{10}\left(\frac{P_i}{P_j}\right), \quad i,j \in \{1,\ldots,U\}. \tag{28}$$

When sorting the received powers by decreasing order, we consider that the power ratio (dB) between two consecutive elements as being constant and equal to PR.

Furthermore, the frequency shifts $\Delta f_i \quad \forall i \in \{1,\ldots,U\}$ are supposed uniformly distributed in $[-\Delta f_{\max}, \Delta f_{\max}]$. The highest frequency offset $\Delta f_{\max}$ is equal to $5\% \times F_s$, with $F_s = (1/T_s)$ is the sampling frequency.[5]

2) Start of Frame Detection: The first step that our receiver has to perform is the detection of the received LoRa-like packets and the identification of the effective start of the frames. Using the coarse and fine synchronization methods as described in Section IV-A, we obtained in Fig. 9 the following curves of the accurate detection probabilities of the start of the frame as a function of the SNR. For each signal, the SNR is defined as

$$\mathrm{SNR} = \frac{P_i}{\sigma_w^2}. \tag{29}$$

Fig. 9 shows that for PR = 6 dB and PR = 3 dB, the start of frame detection of all the received signals is slightly affected compared to the case of a single LoRa packet received without interference. These results prove the immunity of our detection and synchronization (time and frequency) methods against the same SF interference. In addition, a nearly optimal detection is reached for the SNRs greater than −22 dB. Thus, this detection method is consistent with the deployment requirements of the LoRa technology which define the SNR threshold, as presented in Table IV, $\Gamma_{\mathrm{th}}^{(12)} = -20$ dB.

3) SIC Performance: To test the efficiency of our receiver to perfectly synchronize to the strongest signal and remove its contribution, we present in Fig. 10 the evolution of the de-chirped data block. Both spectrograms are obtained before performing the synchronization on the strongest signal in each iteration of our algorithm. Here, we note that in a synchronized mode, each de-chirped LoRa symbol gives constant frequency over the symbol time.

[5] $\Delta f_{\max}$ has been chosen based on the local oscillators precision used for LPWAN applications.

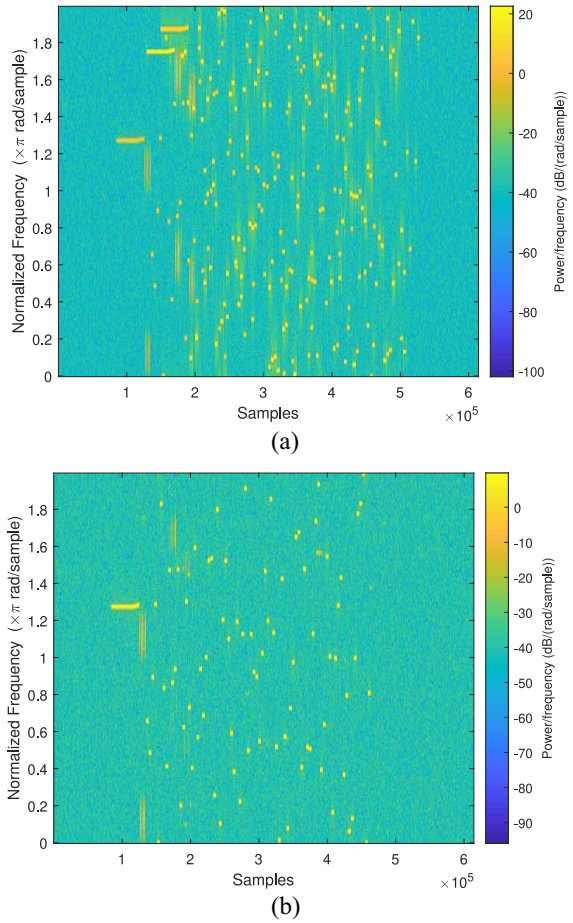

Fig. 10. Evolution of the de-chirped block with PR = 3 dB, SF = 12, and $U = 3$. (a) Initial state. (b) After two iterations.

The spectrogram in Fig. 10(a) represents the initial de-chirped data block where $U = 3$ preambles could be easily identified. We can observe the existence of three long temporal sequences having a constant frequency. Indeed, since the symbols of LoRa preamble have the same value, a constant frequency is obtained over N_p symbol times.

After iterating our algorithm twice, it can be seen in Fig. 10(b) that the contribution of the two signals having the highest received powers is perfectly removed. Hence, our receiver performs accurate time and frequency synchronizations.

4) Decoding Performance: To evaluate the decoding performance of our proposed receiver, we display, in Figs. 11 and 12, the BER evolution of three superposed signals, with PR of 6 and 3 dB, respectively, as a function of the SNR relative to each received signal as depicted in (29).

We note that each dashed curve in both figures represents the BER of a received signal when all steps of our algorithm are performed, except for the processing of superimposed peaks. It can be seen that the decoding performance is enhanced (red and green solid curves) when we implement our algorithm to process the latter critical case.

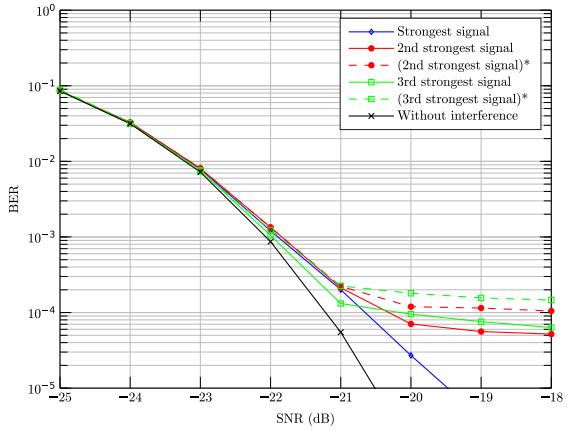

Fig. 11. BER evolution with PR = 6 dB, SF = 12, and $U = 3$.

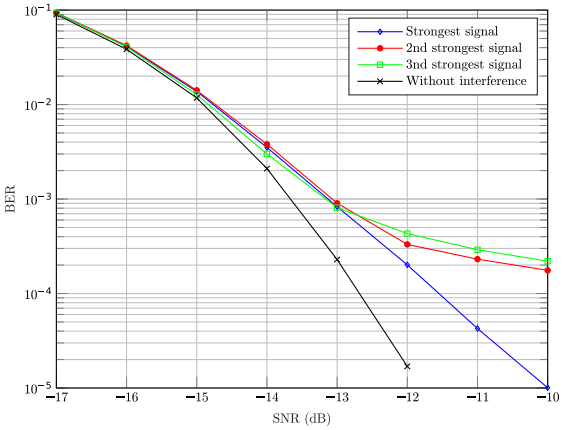

Fig. 13. BER evolution with PR = 6 dB, SF = 9, and $U = 3$.

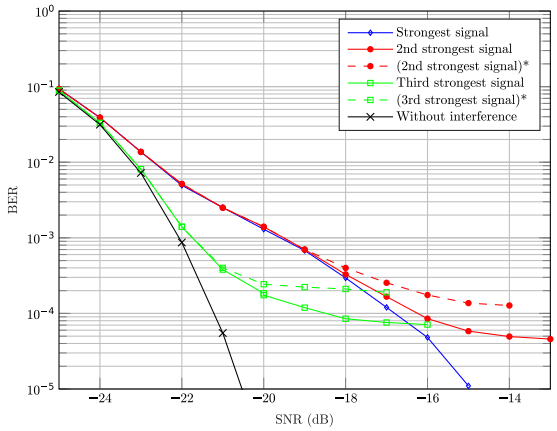

Fig. 12. BER evolution with PR = 3 dB, SF = 12, and $U = 3$.

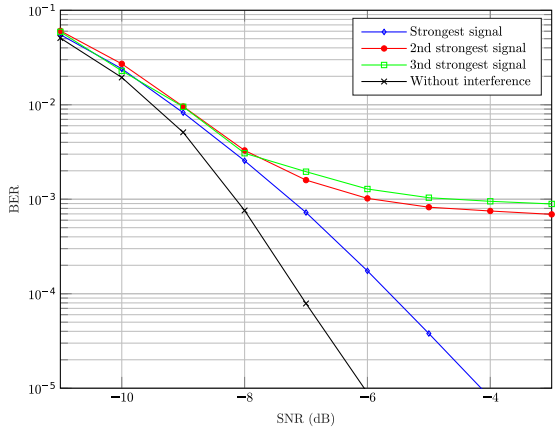

Fig. 14. BER evolution with PR = 6 dB, SF = 7, and $U = 3$.

Furthermore, based on [9], the solid blue curves in both figures show that the decoding performance of the strongest signal is almost identical to the case where only one same SF interfering signal having a received power ratio of 3 and 6 dB is met. This result is explained by the fact that the contribution of the second strongest signal interferes more with the decision of the strongest signal symbols. In addition, we notice that its SNR threshold value, in Fig. 11 (resp. Fig. 12), is increased by almost 1 dB (resp. 5.3 dB) compared to the absence of interference case.

Once the latter signal is decoded, its contribution is removed to process the remaining signals. The solid red curves show that the decoding performance of the second strongest signal is slightly affected by comparing with the BER of the strongest one. But, if the SNR is greater than -20 dB (resp. -15 dB) in Fig 11 (resp. Fig. 12), the BER remains almost constant. These results are explained by:

1) the errors that occur when decoding the strongest signal and removing its contribution;
2) the issue of superimposed peaks which cannot be totally solved;
3) the presence of the third strongest signal as an interfering signal with PR = 6 dB (resp. PR = 3 dB) in Fig. 11 (resp. Fig. 12).

Finally, the receiver has to process the remaining signal. The solid green curves show that the decoding performance of the weakest signal is slightly affected compared to the BER of one LoRa signal without interference. However, with an SNR $= -20$ dB, the BER remains almost constant. These results are also explained by the errors occurring when removing the previous signals. Nevertheless, in this case, the errors introduced by the SIC are more accentuated since two signals are already removed.

Based on the latter results, we can deduce that our receiver can decode accurately three superposed signals with SF = 12 if we guarantee 6 dB as a minimum power ratio between them.

In all the latter simulations, we used SF = 12 which has the longest time on air and is likely to involve collisions [24]. To show the impact of decreasing the SF on the decoding performance of our receiver, we represent in Fig. 13 the BER evolution of the received signals with $SF = 9$. It can be seen that we obtain almost the same results as in Fig. 11 with slight degradation of the decoding performance of the second and the third received signals, which remain acceptable since a BER of 2×10^4 is reached at SNR = 10 dB for both signals. Similarly, in Fig. 14, the latter performance degradation is more accentuated when $U = 3$ superposed signals are received with SF = 7. Indeed, this degradation can be explained by the issue of superposed peaks which is more likely for the lowest SF since the number of points in the FFT is proportional to the SF.

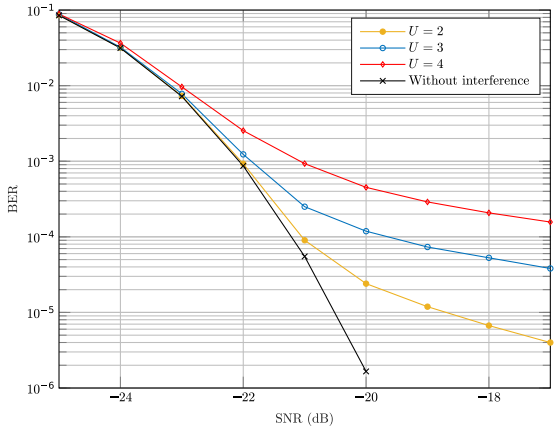

Fig. 15. BER evolution of the weakest signal with $SF = 12$.

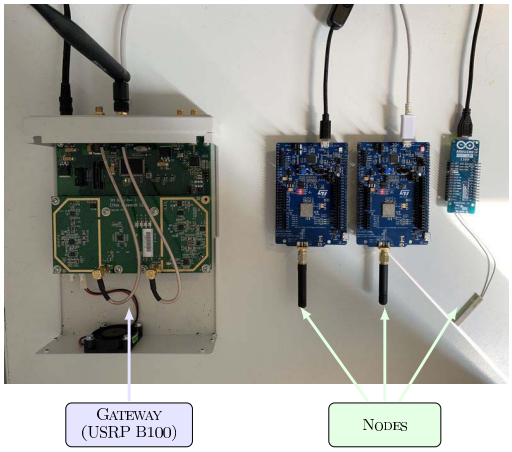

Fig. 16. Test bed: three LoRa node transmitting and one USRP SDR device receiving data.

Thus, our approach is more effective with the highest SF and allows to decode up to four simultaneously received signals as presented in the next simulation.

The final simulation test is to evaluate the impact of increasing the number of superposed signals on the decoding performance of our receiver. To this end, we represent in Fig. 15 the BER evolution of the weakest received signal during T_B. Here, we assumed that PR is uniformly distributed in $[6, 10]$ dB. In such a configuration, we notice that for $U = 2$, the weakest signal is effectively decoded since at the SNR threshold $\Gamma_{\text{th}}^{(SF=12)}$, the BER is equal to 2×10^{-5}. However, given that errors in decoding the synchronized signal are spread over the residual signals at each iteration, the decoding performance of the weakest signal is more degraded for $U \in \{3, 4\}$. Nevertheless, the latter performance remains acceptable since a BER of 10^{-4} is reached at $\Gamma_{\text{th}}^{(SF=12)}$ for $U = 3$ and a BER of 2×10^{-4} is reached for $U = 4$ at SNR $= -18$ dB.

B. Experimental Validation

In this section, we aim to validate our simulation results by considering real LoRa deployments. To that end, we use our own-made LoRa nodes and gateways as represented in Fig. 16 and detailed in [25].

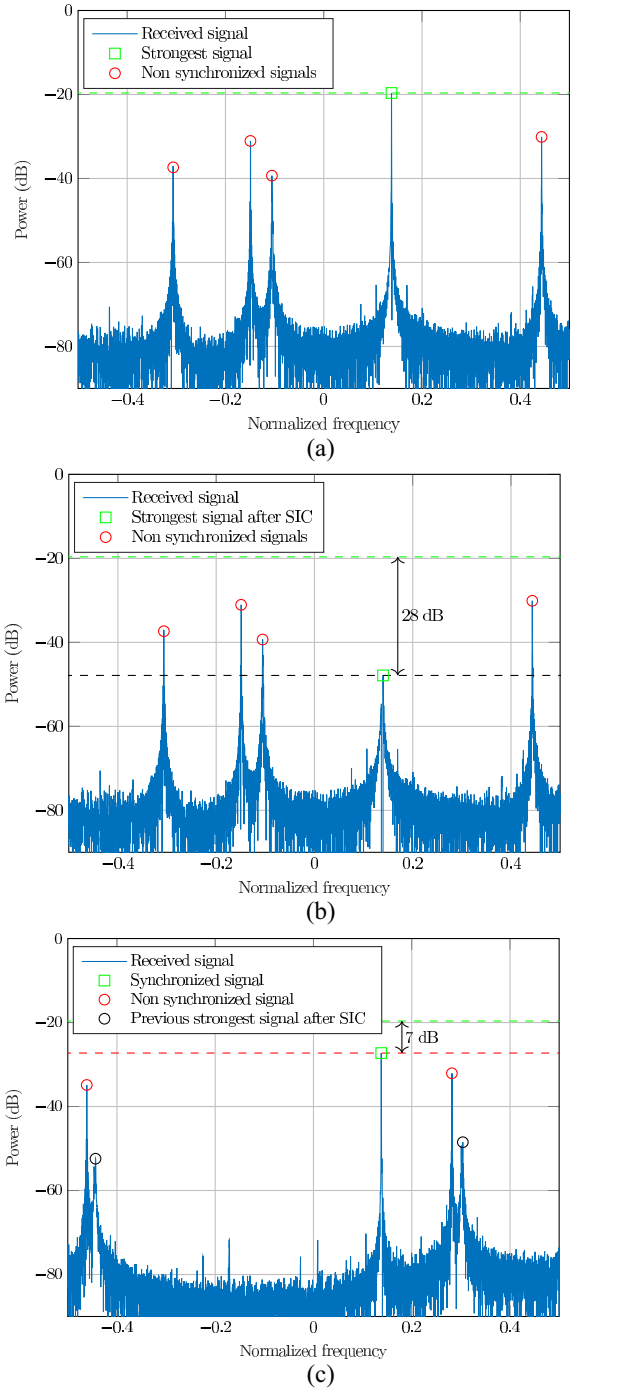

Fig. 17. Result of the FFT. (a) Synchronization on the strongest signal. (b) Strongest signal cancellation. (c) Synchronization on the second strongest signal.

Three LoRa nodes ($U = 3$) are configured to transmit continuously, with the same SF (here SF $= 12$), the same message every second with a constant power ratio $PR = 6$ dB. Thus, a high probability of collision between LoRa signals is obtained. All the nodes send data at a 868.2-MHz carrier frequency with a bandwidth $B = 125$ kHz. We also use software-defined radios (SDR) universal software radio peripheral (USRP) B100 [26] to acquire and process the data.

In order to estimate the noise level detected by the receiver (i.e., compute σ_w^2), we start the acquisition on the reception

side when the nodes are not transmitting. Then, we start the transmission of all the nodes randomly without any previous timing synchronization. To maintain the same power ratio between received signals as configured in the nodes, the latter is placed at the same distance from the USRP.

Fig. 17 presents the result of the FFT processing in the pth T-long section, where $U_p = 3$. It represents the capability of our receiver to synchronize on the strongest signal in each iteration and to remove its contribution to process the remaining signals.

The spectrum in Fig. 14(a) shows that with real LoRa signals, it is difficult to obtain a perfect Dirac for the synchronized signal as in the theory. We also notice that this spectrum is consistent with (22), where each nonsynchronized signal contributes with two cardinal sines.

Furthermore, as we can see in Fig. 17(b), the contribution of the strongest signal is not perfectly removed but dramatically reduced by 28 dB. This proves that our receiver efficiently performs time and frequency synchronizations and estimates accurately the frequency, the magnitude, and the phase of the latter signal in each T-long section.

Once the contribution of the latter signal is removed, the receiver performs time and the frequency synchronizations on the signal having the second highest received power. In Fig. 17(c), it can be seen that the power ratio between the latter two signals is 7 dB, which is almost equal to the power ratio configured on the transmitting nodes since they are equidistant to the USRP. In addition, removing the contribution of the synchronized signal by almost 28 dB provides a good margin to process the remaining ones.

Finally, thanks to our approach, we were able to synchronize (time and frequency synchronizations) and decode the signal information from the three nodes. This interesting performance would increase considerably the capacity of LoRa technology-based networks, enhance the spectral efficiency, and reduce the energy consumption of the nodes.

VI. Conclusion

With the exponential growth of the number of connected objects, packet collisions are becoming a challenge for the IoT systems. In LoRa communication, the use of RACH to avoid the collisions is far from ideal. Therefore, in this article, we proposed the design of a receiver capable to process destructive LoRa-like collisions. Indeed, we showed through mathematical models, simulation results, and experimental validation that simultaneously received LoRa-like signals with the same SF could be processed and we were able to extract the information from the transmitting nodes. As a result, our novel approach would reduce the energy consumption of the nodes and enhance the capacity of LoRa technology-based networks since it decreases the number of retransmitted packets.

Our solution has also the advantage of using the commercialized LoRa chip to process collisions. Thus, it can be easily implemented to an existing network to enhance spectral efficiency. As future work, a complete link and system-level simulator would be developed to outline the benefits of the proposed approach in a real-world scenario in terms of throughput and energy consumption. Indeed, the same and different SF interference would be considered, as well as the interference from other technologies in ISM bands. Moreover, we are planning to enhance the processing for the lowest SF in order to deal with the issue of superposed peaks.

Acknowledgment

The authors would like to thank F. Le Neindre and M. Rezzouki for their insights and help in managing the USRP SDR devices and LoRa nodes.

References

[1] IoT Analytics GmbH. (2018). *State of the IoT and Short-Term Outlook*. [Online]. Available: https://iot-analytics.com/product/state-of-the-iot-2018/

[2] Semtech. (2013). *LoRa Modem Design Guide: Sx1272/3/6/7/8*. [Online]. Available: https://www.semtech.com/uploads/documents/LoraDesignGuide_STD.pdf

[3] "Low power long range transmitter," U.S. Patent 20 140 219 329 A1, Jan. 2014. [Online]. Available: https://patents.google.com/patent/US20140219329A1/en

[4] L. Vangelista, "Frequency shift chirp modulation: The LoRa modulation," *IEEE Signal Process. Lett.*, vol. 24, no. 12, pp. 1818–1821, Dec. 2017.

[5] B. Reynders and S. Pollin, "Chirp spread spectrum as a modulation technique for long range communication," in *Proc. Symp. Commun. Veh. Technol. (SCVT)*, Nov. 2016, pp. 1–5.

[6] LoRa Alliance, (2017). *LoRaWAN—Specification V1.1*. [Online]. Available: https://lora-alliance.org/resource-hub/lorawanr-specification-v11

[7] M. Ni, M. Jafarizadeh, and R. Zheng, "On the effect of multi-packet reception on redundant gateways in LoRaWANs," in *Proc. IEEE Int. Conf. Commun. (ICC)*, May 2019, pp. 1–6.

[8] T. Elshabrawy and J. Robert, "Analysis of BER and coverage performance of LoRa modulation under same spreading factor Interference," in *Proc. IEEE 29th Annu. Int. Symp. Pers. Indoor Mobile Radio Commun. (PIMRC)*, Sep. 2018, pp. 1–6.

[9] O. Afisiadis, M. Cotting, A. P. Burg, and A. Balatsoukas-Stimming, "LoRa symbol error rate under non-chip- and non-phase-aligned interference," 2019. [Online]. Available: arXiv.abs/1905.00439.

[10] D. Croce, M. Gucciardo, S. Mangione, G. Santaromita, and I. Tinnirello, "Impact of LoRa imperfect orthogonality: Analysis of link-level performance," *IEEE Commun. Lett.*, vol. 22, no. 4, pp. 796–799, Apr. 2018.

[11] J. Markkula, K. Mikhaylov, and J. Haapola, "Simulating LoRaWAN: On importance of inter spreading factor interference and collision effect," in *Proc. IEEE Int. Conf. Commun. (ICC)*, May 2019, pp. 1–7.

[12] U. Noreen, L. Clavier, and A. Bounceur, "LoRa-like CSS-based PHY layer, capture effect and serial interference cancellation," in *Proc. 24th Eur. Wireless Conf.*, May 2018, pp. 1–6.

[13] N. E. Rachkidy, A. Guitton, and M. Kaneko. (2018). *Decoding Superposed LoRa Signals*. [Online]. Available: http://arxiv.org/abs/1804.00503

[14] B. Laporte-Fauret, M. A. Ben Temim, G. Ferré, D. Dallet, B. Minger, and L. Fuché, "An enhanced LoRa-Like receiver for the simultaneous reception of two interfering signals," in *Proc. IEEE 30th Annu. Int. Symp. Pers. Indoor Mobile Radio Commun. (PIMRC)*, Sep. 2019, pp. 1–6.

[15] M. Chiani and A. Elzanaty, "On the LoRa modulation for IoT: Waveform properties and spectral analysis," 2019. [Online]. Available: http://arxiv.org/abs/1906.04256

[16] T. Elshabrawy and J. Robert, "Interleaved chirp spreading LoRa-based modulation," *IEEE Internet Things J.*, vol. 6, no. 2, pp. 3855–3863, Apr. 2019.

[17] R. Ghanaatian, O. Afisiadis, M. Cotting, and A. Burg. (2018). *LoRa Digital Receiver Analysis and Implementation*, [Online]. Available: http://arxiv.org/abs/1811.04146

[18] V. Talla, M. Hessar, B. Kellogg, A. Najafi, J. R. Smith, and S. Gollakota, "LoRa backscatter: Enabling the vision of ubiquitous connectivity," *Proc. ACM Interact. Mobile Wearable Ubiquitous Technol.*, vol. 1, no. 3, pp. 1–24, Sep. 2017. [Online]. Available: http://doi.acm.org/10.1145/3130970

[19] J. C. Liando, A. Gamage, A. W. Tengourtius, and M. Li, "Known and unknown facts of LoRa: Experiences from a large-scale measurement study," *ACM Trans. Sensor Netw.*, vol. 15, no. 2, pp. 1–35, Feb. 2019. [Online]. Available: http://doi.acm.org/10.1145/3293534

[20] *Communication Systems*. (Jan. 2016). [Online]. Available: https://patents.google.com/patent/EP2449690B1/en
[21] G. Colavolpe, T. Foggi, M. Ricciulli, Y. Zanettini, and J. Mediano-Alameda, "Reception of LoRa signals from LEO satellites," *IEEE Trans. Aerosp. Electron. Syst.*, vol. 55, no. 6, pp. 3587–3602, Dec. 2019.
[22] G. Ferré and A. Giremus, "LoRa physical layer principle and performance analysis," in *Proc. 25th IEEE Int. Conf. Electron. Circuits Syst. (ICECS)*, Dec. 2018, pp. 65–68.
[23] M. Knight and B. Seeber, "Decoding LoRa: Realizing a modern LPWAN with SDR," in *Proc. GNU Radio Conf.*, vol. 1, 2016, pp. 1–5. [Online]. Available: https://pubs.gnuradio.org/index.php/grcon/article/view/8
[24] G. Ferré and E. P. Simon, "Packet collision analysis when heterogeneous unlicensed IoT technologies coexist," *IET Netw.*, vol. 7, no. 6, pp. 384–392, Nov. 2018. [Online]. Available: http://digital-library.theiet.org/content/journals/10.1049/iet-net.2018.0026
[25] G. Ferré, F. Rivet, R. Tajan, and E. Kerhervé, "Design and deployment of an IoT network based on LoRa," in *Proc. Eur. Assoc. Educ. Elect. Inf. Eng. (EAEEIE)*, Grenoble, France, Jun. 2017, pp. 1–6.
[26] Ettus Knowledge Base. (2016). *B100—Ettus Knowledge Base*. [Online]. Available: https://kb.ettus.com/index.php?title=B100&oldid=2983

Mohamed Amine Ben Temim (Student Member, IEEE) received the degree in telecommunication engineering from the Higher School of Communication of Tunis (Sup'Com), University of Carthage, Tunis, Tunisia, in 2018. He is currently pursuing the Ph.D. degree in Internet of Things in order to propose solution for interference issues with the IMS Laboratory, University of Bordeaux, Bordeaux, France.

He has authored three papers in national and international conferences.

Mr. Ben Temim received the Best Paper Award at the IEEE International Symposium on Personal, Indoor and Mobile Radio Communications in 2019, Track 4, titled "An Enhanced LoRa-Like Receiver for the Simultaneous Reception of Two Interfering Signals."

Guillaume Ferré (Member, IEEE) received the degree in electronic and telecommunication engineering (ENSIL) from the University of Limoges, Limoges, France, in 2003, and the Ph.D. degree in digital communications and signal processing from the Limoges University of Technology, Limoges, in 2006.

From 2006 to 2008, he was a Postdoctoral Researcher with the Limoges XLIM Laboratory and then with the IMS Laboratory, University of Bordeaux, Bordeaux, France. Since 2008, he has been an Associate Professor with Ecole Nationale Supérieure d'Electronique, d'Informatique, Télécommunications, Mathématique et Mécanique (ENSEIRB-MATMECA), Talence, France, an engineering school of Bordeaux INP. After several administrative responsibilities in the Telecommunications Department of ENSEIRB-MATMECA. He is currently the Director of Industrial Relations. He has authored more than 100 papers in international conferences. He is the Principal Investigator of many national and international projects, at the local level he is responsible for two research activities related to IoT, including one to investigate on the smart campus. He has also authored four patents. He currently supervises five Ph.D. students with a significant part of industrial research activities. He carries out his research activities within the IMS Laboratory in the "signal and image" team. These fields of research concern the circuits and systems for digital communications, it includes: signal processing and digital communications for 5G; and digital enhancement for wideband power amplifiers and time interleaved analog-to-digital converters.

Dr. Ferré received the Best Paper Award at the IEEE International Symposium on Personal, Indoor and Mobile Radio Communications in 2019, Track 4, titled "An Enhanced LoRa-Like Receiver for the Simultaneous Reception of Two Interfering Signals." In the IMS Laboratory, he holds the position of the Vice-President of the Scientific Council. He is a member of several Technical Program Committees, such as ICT and ICECS.

Baptiste Laporte-Fauret (Graduate Student Member, IEEE) received the degree in electronic and telecommunication engineering from the Ecole Nationale Supérieure d'Electronique, d'Informatique, Télécommunications, Mathématique et Mécanique (ENSEIRB-MATMECA) of Bordeaux, Bordeaux INP, Talence, France, in 2017. He is currently pursuing the Ph.D. degree in analog-to-digital converters in order to enhance their bounded dynamic range with the IMS Laboratory, University of Bordeaux, Bordeaux, France, in partnership with the French company Thales, France.

He is currently an author of eight papers in proceedings of peer-reviewed international and national conferences and one industrial patent.

Mr. Laporte-Fauret received the Best Paper Award at the IEEE International Symposium on Personal, Indoor and Mobile Radio Communications in 2019, Track 4, titled "An Enhanced LoRa-Like Receiver for the Simultaneous Reception of Two Interfering Signals." Since 2019, he has been the Co-Chair of the Instrumentation and Measurement IEEE student branch of the IMS Laboratory.

Dominique Dallet (Member, IEEE) received the Ph.D. degree in electrical engineering from the University of Bordeaux, Talence, France, in 1995.

From 2010 to 2013, he was the Head of the Electronic Embedded System Department. He is currently the Head of the Electronic Design Group, IMS Laboratory, University of Bordeaux. He is currently a Full Professor of digital electronic design with the Engineer School Bordeaux INP, and he is doing his research with the IMS Laboratory (Laboratoire de l'Intégration du Matériau au Système, Bordeaux INP, University of Bordeaux CNRS UMR 5218). He has authored over 200 papers in international and national journals or in proceedings of peer-reviewed international conferences, book chapters, and patents. His current research interests include data converter (A/D-D/A) modeling and testing, parameter estimation, digital signal processing implementation in different targets (application-specified integrated circuit and field-programmable gate array), and electronic design for the digital enhancement of analog and mixed electronic circuits (ADC, DAC, and power amplifier).

Dr. Dallet received the IstvánKollár Award for the Best Paper presented at IMEKO-TC4 2016 Symposium, titled "Accurate Sine-Wave Frequency Estimation by Means of an Interpolated DTFT Algorithm" for his coauthored paper. Since 2015, he has been the Chairperson with the Technical Committee "Measurement of Electrical Quantities"-IMEKO TC4.

Bryce Minger received the degree in telecommunications engineering from the Ecole Nationale Supérieure d'Electronique, d'Informatique, Télécommunications, Mathématique et Mécanique (ENSEIRB-MATMECA) of Bordeaux, Bordeaux INP, Talence, France, in 2013, and the Ph.D. degree in digital communications and signal processing from the University of Bordeaux in collaboration with Thales, France, in 2017.

He is currently a Signal Processing Research and Development Engineer of digitized RF systems with Thales. He has authored several patents, papers in proceedings of peer-reviewed international conferences or international journals, and one book chapter. He is also involved in the industrial supervision of one Ph.D. student. In addition to its scientific activities, he has been a young auditor of the French Institute for Higher National Defence Studies since 2019. His current research domain focuses on the enhancement of radio equipment by means of digital signal processing. This includes modeling, testing, and post-distortion of data converters, and digital signal processing implementation on field-programmable gate array and power amplifier predistortion.

Loïc Fuché received the Ph.D. degree in electrical engineering from the University of CAEN, Caen, France, in 1990.

In 1991, he joined Thomson CSF/RGS (currently, Thales-SIX), France, as an Engineer in the field of digitalized RF. He has authored or coauthored ten patents. His current research domain focuses on the architecture of digitized radio equipment and more specifically on the functions to improve radio performance.